JMEPEG (2012) 21:756–763
DOI: 10.1007/s11665-012-0199-y

1059-9495/$19.00

SintClad: A New Approach for the Production of Wear-Resistant Tools

M. Blüm, H. Hill, H. Moll, S. Weber, and W. Theisen

(Submitted October 13, 2011; in revised form January 24, 2012)

Tools used in the mineral processing industry are required to feature high wear resistance to facilitate an adequate cost efficiency. These kinds of tools are made of composite materials based on a low-alloyed substrate material and a high-alloyed coating. The coatings can be applied in different ways using production processes like HIP cladding, deposit welding, and composite casting. The article is concerned with the problem of a novel and cost-effective coating alternative: sinter cladding, using the principle of super-solidus liquid-phase sintering (SLPS). Usually SLPS represents a sintering technique, which is used for the compaction of high-alloyed metal powders. However, no recognizable efforts were made to use the SLPS-process for applying a PM-coating on a bulk substrate material. Sinter cladding for the first time uses SLPS to combine the process of powder compaction with the application of a coating to a solid steel substrate into one single step. Another advantage of the process is the possibility to produce massive bulk coatings with thicknesses exceeding 20 mm. This article is original in the scope of question and investigation methods in terms of microstructure, hardness profiles, EDX measurements, diffusion calculations, and computational thermodynamics.

Keywords computational thermodynamics, diffusion calculations, powder metallurgy, super-solidus liquid-phase sintering (SLPS), thick coatings

1. Introduction

Mineral processing demands highly wear-resistant tools (Ref 1), which in most cases are also subjected to dynamic loads. Modern approaches suffice these opposing requirements of both high hardness and at the same time high toughness by a composite concept consisting of a tough substrate material with a wear-resistant coating. Common fabrication methods to apply such coatings are composite casting (Ref 2, 3), deposit welding (Ref 4), or HIP cladding (Ref 5). Composite casting and deposit welding are quite fast and cheap methods, but suffer from thermodynamic restrictions and an inhomogeneous hard phase distribution compared with the coatings obtained by HIP. Several investigations proved the usability of HIP cladding (Ref 6, 7) for the production of metal matrix composite (MMC) coatings. However, due to complex encapsulation and the dependence on special HIP furnaces, HIP also proved to be a rather expensive and inflexible process technology. Hence, the demand for alternative production processes is still high. Such an alternative process should exhibit a PM like microstructure and offer short processing times using common techniques to ensure cost effectiveness. One promising way can be found in super-solidus liquid-phase sintering (SLPS), a principle which has been under research in recent years in connection with pre-alloyed tool steels (Ref 8–12) and MMC (Ref 11–13).

From the economical point of view, SLPS offers some advantages compared with HIP, such as a shorter consolidation time, none or reduced encapsulation requirements, as well as reduced requirements on the furnace. All of those lead to a higher cost efficiency of the process. SLPS of high-alloyed steels takes place in the temperature interval between solidus and liquidus temperatures generating a liquid-phase fraction of 20-40% (Ref 14). The consolidation process starts with the formation of liquid phase along the grain boundaries to allow a viscous flow (Ref 15). Wetting of the particle interfaces and separation into smaller particles occur as the amount of liquid phase increases. The last step of densification involves capillary forces that lead to a rearrangement of the powder particles (Ref 15). Nevertheless, when used as a coating technology, several questions arise, which bring a significant amount of complexity into the system. Starting from SLPS of a single high-alloyed metal powder, it is possible to determine an optimal sintering temperature generating exactly the amount of liquid phase required for densification. Shifting the optimal sinter window to higher temperatures leads to an increased coarsening of the microstructure, whereas lower temperatures result in unwanted residual porosity (Ref 14). It becomes more complex with the presence of another material, in this case a low-alloyed substrate material. Although SLPS dwell time of only a few minutes is aspired, it can be estimated that diffusion processes between powder and substrate take place. In the presence of

This article is an invited submission to JMEP selected from presentations at the Symposia "Wetting, soldering and brazing" and "Diffusion bonding and characterization" belonging to the Topic "Joining" at the European Congress and Exhibition on Advanced Materials and Processes (EUROMAT 2011), held September 12-15, 2011, in Montpellier, France, and has been expanded from the original presentation.

M. Blüm, H. Hill, H. Moll, S. Weber, and **W. Theisen**, Ruhr-Universität Bochum—Lehrstuhl für Werkstofftechnik, Universitätsstr. 150 Gebäude IA 2/39, 44780 Bochum, Germany. Contact e-mail: bluem@wtech.rub.de.

liquid phase, diffusion processes between cladding material and substrate may run at higher speed, due to the higher diffusion coefficient in liquid phase. Therefore, several investigations on the diffusion of elements were carried out to analyze the diffusion zone. Based on these results, the influence of the diffusion processes on the liquid phase content was investigated. This would have an effect on the optimum SLPS parameters and thereby on the resulting microstructure of the bulk coating. Finally, this study evaluates the potential of the novel aspect to utilize SLPS for cladding applications.

2. Experimental

2.1 Materials

As coating material, a gas-atomized PM cold work tool steel X245VCrMo9-4 (X245) was used. In the as-sintered state, its microstructure features a high amount of vanadium-rich MC carbides in a metal matrix (Ref 11) (see Fig. 1). For the Sinter Cladding experiments, a common construction steel of grade S355 was used as substrate. While the cold work tool steel was available in gas-atomized state, the substrate samples were cut from a strip-casted bar stock and subsequently abraded by SiC paper (Mesh 80), and cleaned with ethanol. After sintering, the chemical composition of coating and substrate material was measured by spark spectroscopy (type: QSG750, company: OBLF). The results are given in Table 1.

2.2 Processing

The sintering was carried out in a vacuum furnace that can be heated up to a maximum temperature of 1350 °C. The vacuum system allows a pressure of 1×10^{-1} Pa at room temperature.

The experimental setup is sketched in Fig. 2. It consists of an alumina crucible which is filled with coating powder. The powder is pre-compacted to tap density, and the substrate material is placed on top of the coating powder. During the sintering process, the substrate is intended to sink into the partially liquefied powder by its own weight.

The bolt, depicted in Fig. 2, limits the maximum sink depth of the substrate defining the designated thickness of the coating, which was designated to 20 mm in this study. The following processing sequences were used for the sinter experiments:

- Evacuation of the vacuum chamber to a pressure of 1×10^{-1} Pa.
- Heating to 300 °C with a heating rate of 10 K/min.
- Dwell of 30 min at 300 °C to remove residual adsorbed gaseous species.
- Heating to sintering temperature at a heating rate of 10 K/min.
- Dwell of 30 min at sintering temperature.
- Slow cooling at a cooling rate of 5 K/min to 800 °C
- Free cooling in the furnace with a t8 = 5-time of about 50 min.

2.3 Microstructure

For all microstructural investigations, samples were cut off from the sintered parts and mounted in a conductive polymer resin. Subsequently, they were ground on SiC paper and polished with 6-, 3-, and 1-µm diamond suspension. For final preparation, a SiO_2 suspension with a particle size of 0.25 µm was used. Etching was applied using the "V2A" etchant (Ref 16). The microstructures were investigated by optical microscopy (OM) and scanning electron microscopy (SEM). OM was applied to check residual porosity and the homogeneity of the microstructure in the whole cross section. For investigations at higher magnifications and local chemical analysis by energy

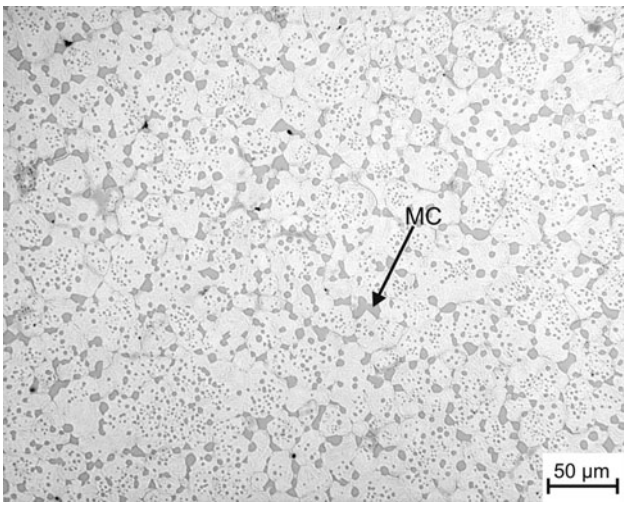

Fig. 1 Microstructure of X245 after sintering at 1280 °C and a dwell of 30 min

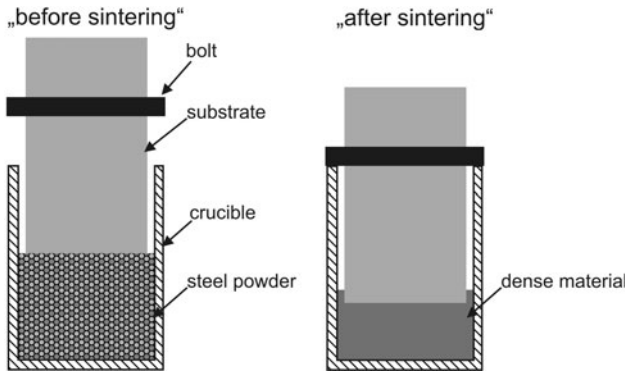

Fig. 2 Experimental setup for the bond sintering tests

Table 1 Chemical compositions of the material; values are given in mass.% with iron being the dependent substitutional element

	C	Cr	Mo	Ni	V	W	Si	Mn
X245	2.547 ± 0.0515	4.08 ± 0.003	3.51 ± 0.005	0.171 ± 0.0005	9.61 ± 0.1165	0.88 ± 0.005	0.446 ± 0.0105	0.446 ± 0.0105
S355	0.193 ± 0.029	0.114 ± 0.006	0.03 ± 0.001	0.145 ± 0.001	0.005 ± 0.0005	0.011 ± 0.001	0.37 ± 0.0215	1.085 ± 0.0025

dispersive x-ray analysis (EDX), the SEM was used. The SEM was operated at an accelerating voltage of 20 kV and a working distance of 39 mm.

The density of the cladding material was measured via image analysis using a threshold binarization method of images taken by an optical microscope at a magnification of 200:1. Every given value is the average of at least five different images of the same sample.

2.4 Hardness Profiles

To determine the reactions between the high- and low-alloyed materials, hardness profiles of the sintered bonds were performed according to DIN EN ISO 6507-1 via Vickers method (Ref 17). For a coarse overview, a hardness profile was created using a macrohardness (HV30) tester (type: DiaTestor2n, company: Wolpert), while a microhardness (HV0.05) tester (type: MHT-10, company: Anton Paar) was used to investigate the diffusion zone. All the values were calculated as arithmetic means of five parallel hardness profiles.

2.5 Diffusion Calculations and Computational Thermodynamics

For calculating the diffusion profiles between coating and substrate, the software package DIffusion-Controlled TRAnsformations (DICTRA) (Ref 18–20) version 23 and the database Mob2 (Ref 21), providing mobility data of elements in different phases (Ref 22–24), was used. In addition, the database TCFe4 was applied in DICTRA providing the thermodynamic data. The calculations were carried out isothermally at 1280 °C using a one-dimensional region of 10 mm in width. This region was symmetrically divided into two parts using the heavy-side step function, hs(x). The substrate material is fully austenitic in this condition, while the cold work tool steel exhibits an austenitic matrix in equilibrium with vanadium-rich mono carbides and liquid phase. MC and liquid phase were included in the DICTRA simulation using the model for dispersed phases and calculating their volume fractions in forefront of the diffusion calculation as equilibrium phases. A grid consisting of 100 points and a higher point density towards the interface was defined, while the simulation time was set to 30 min to consider the dwell time of the sintering process.

In addition, the diffusion calculations were supported by thermodynamic calculations by means of Thermo-Calc version R and the TCFe6 database (Thermo-Calc AB, Stockholm, Sweden). Using Thermo-Calc, the liquid phase/carbon-concentration isopleths were calculated without a phase-set reduction.

3. Results and Discussion

3.1 Microstructure

According to Fig. 3, the density of the X245-coating increases with the sintering temperature reaching almost complete densification. After sintering at 1280 °C, the microstructure shows small vanadium-rich carbides and high porosity next to the boundary layer (see Fig. 4a). Increasing the sintering temperature to 1300 °C results in an almost dense microstructure with a lower quantity of carbides (Fig. 4b). The carbide size is increased by Ostwald ripening, keeping the total carbide volume fraction constant. After sintering at 1320 °C

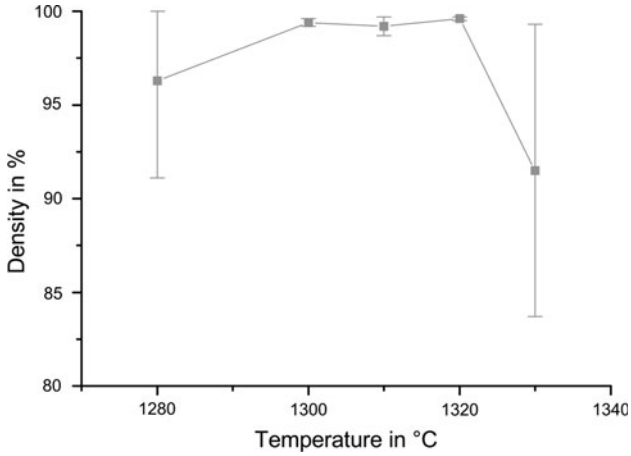

Fig. 3 Density of X245 after sinter cladding at different temperatures

(Fig. 4c), a formation of network-like carbide structures along the grain boundaries can be recognized. This finding corresponds to earlier results showing that sintering at higher temperatures promotes the formation of carbide networks on account of the increased amount of liquid phase (Ref 8, 12). Sintering temperatures higher than 1330 °C with dwell times of 30 min lead to a cast-like microstructure (Fig. 4d), due to an excess of liquid phase.

Figure 5 gives an overview of the microstructure in substrate and coating after sintering at 1300 °C with a dwell time of 30 min. Close to the boundary layer, the construction steel reveals a primarily perlitic microstructure (see Fig. 6) changing to a mixture of ferrite and perlite in greater distance. The cladding material shows next to the boundary layer a carbide-free diffusion zone of 10 µm thickness. To have a detailed look on these microstructural changes close to the boundary, microhardness measurements were used.

3.2 Hardness Profiles

The hardness measurement of the prementioned sample (sintered at 1300 °C; Fig. 7) reveals a nearly constant hardness of about 700 HV30 in the coating. This decreases to 630 ± 10 HV30 at a distance of 1 mm to the interface. Coming from the coating, in a distance of 1 mm in direction of the substrate, there is an increase in hardness of 40 HV30.

The microhardness results (see Fig. 8) reveal a more pronounced gradient in the boundary zone. Owing to the scatter of the measured hardness, and the influence of the MC segregations on the hardness, the measured values were linked by fitted curves. On the coatings side of the boundary, the Boltzmann fits indicate that the hardness begins to drop in a distance of approximately 150 µm from the boundary. On the substrate side, a value of 300 ± 12 HV0.05 was measured directly at the boundary layer, dropping rapidly to about 250 ± 12 HV0.05 in −50-µm and 200 ± 17 HV0.05 in −2000-µm distance within the substrate material. This indicates that close to the boundary layer, a distinct diffusion of elements, which are able to increase the hardness, took place.

3.3 EDX Measurements

For further investigations of the diffusion reactions of the major alloying elements like chromium, molybdenum, and

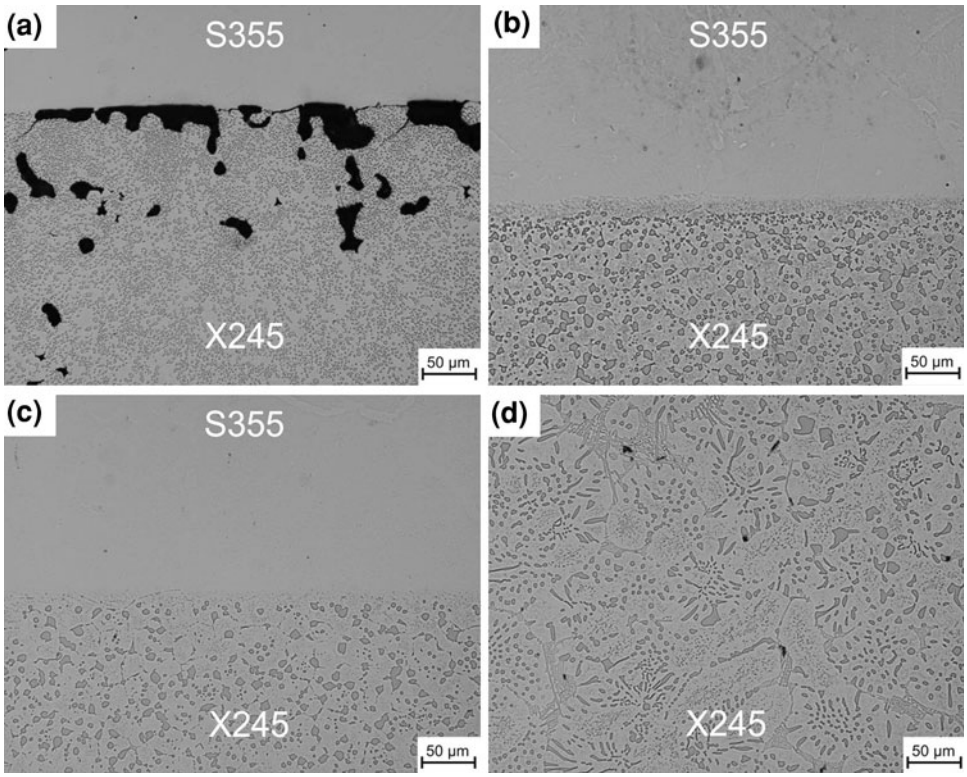

Fig. 4 Microstructure of the sintered bonds X245/S355 (a) 1280 °C, 30 min (b) 1300 °C, 30 min (c) 1320 °C, 30 min, (d) 1330 °C, 30 min

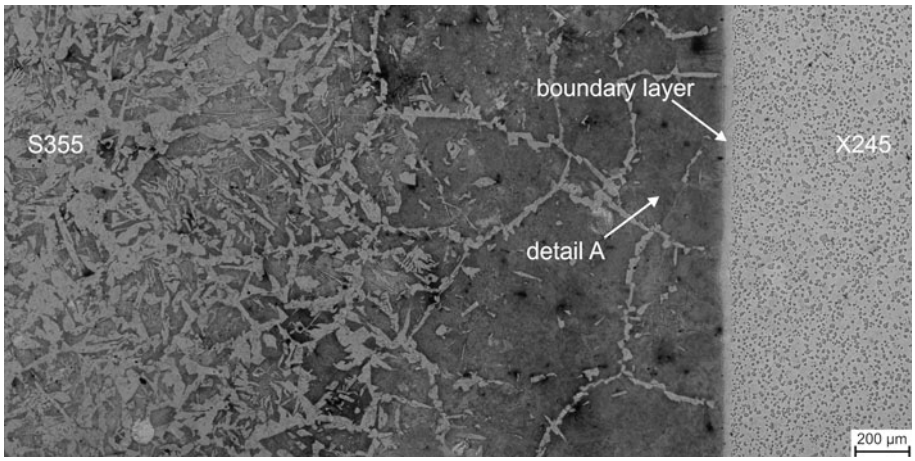

Fig. 5 Microstructure of the bond X245/S355 sintering at a temperature of 1300 °C with a dwell of 30 min; etched with "V2A"-etchant

vanadium EDX linescans were performed (Fig. 9). The linescans revealed no sharp boundary line between both materials. The sharp peaks visible in the linescans of molybdenum and vanadium can be related to the measurement of carbides within the coating material. Therefore, Boltzmann fits were performed to compensate their effect on the calculated mean element content soluted in the metallic matrix. A distinct chromium diffusion is visible from the high (about 4 mass.% Cr)- to the low-alloyed (about 0.5 mass.% Cr) steel, as the result of a strong gradient of the chemical potential (Ref 20). Hence, a diffusion of molybdenum also appears which is less distinct compared to chromium because of the minor driving force due to lower difference in concentration in the chemical compositions (see Table 1). The diffusion of these elements leads to a deceleration of ferrite formation and a solid solution strengthening, whereby the hardness is increased in this area (Ref 25), which correlates to the measured microhardness profile (see Fig. 8). In the case of vanadium, the diffusion activity is comparatively low. Although the total amount of vanadium in the X245 exceeds that of chromium and molybdenum, the dissolved amount in the matrix is lower due to the strong formation of vanadium-rich mono carbides (Ref 11). The mean value of molybdenum equates to 3.55 mass.% dissolved in the metal matrix, and in the case of vanadium, there is an average

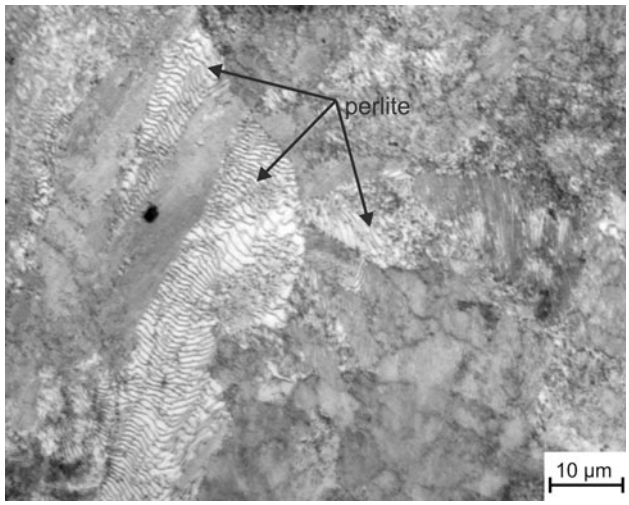

Fig. 6 Detail A of Fig. 5

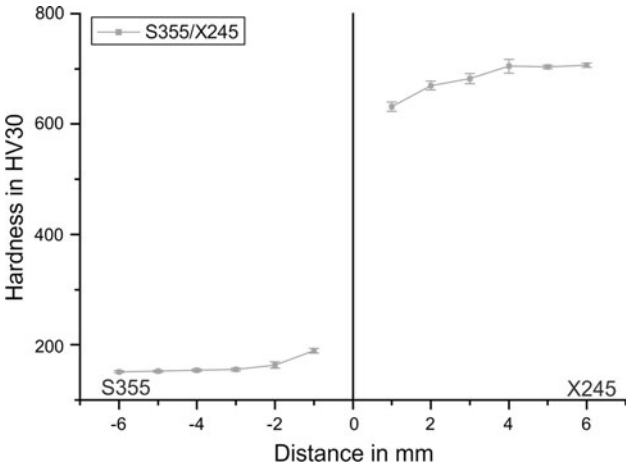

Fig. 7 Macrohardness profile of the bond between coating and substrate materials with a length of 12 mm

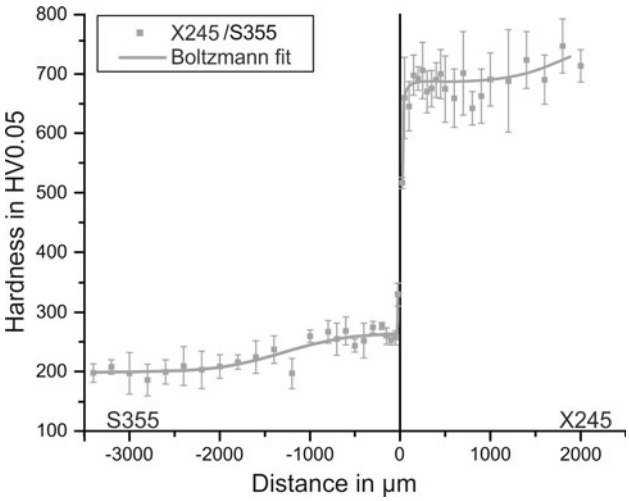

Fig. 8 Microhardness profile of the bond between coating and substrate materials with a length of 5.5 mm

of 1.6 mass.%. However, the distinct increase in hardness and the strong formation of pearlite cannot be explained by the diffusion of these substitutional elements. It is assumed that also a carbon diffusion took place. However, it is impossible to quantify the carbon diffusion by EDX due to the low atomic order of carbon. Therefore, diffusion calculations were necessary, to gain knowledge about the diffusion of carbon and its effect on the measured hardness values.

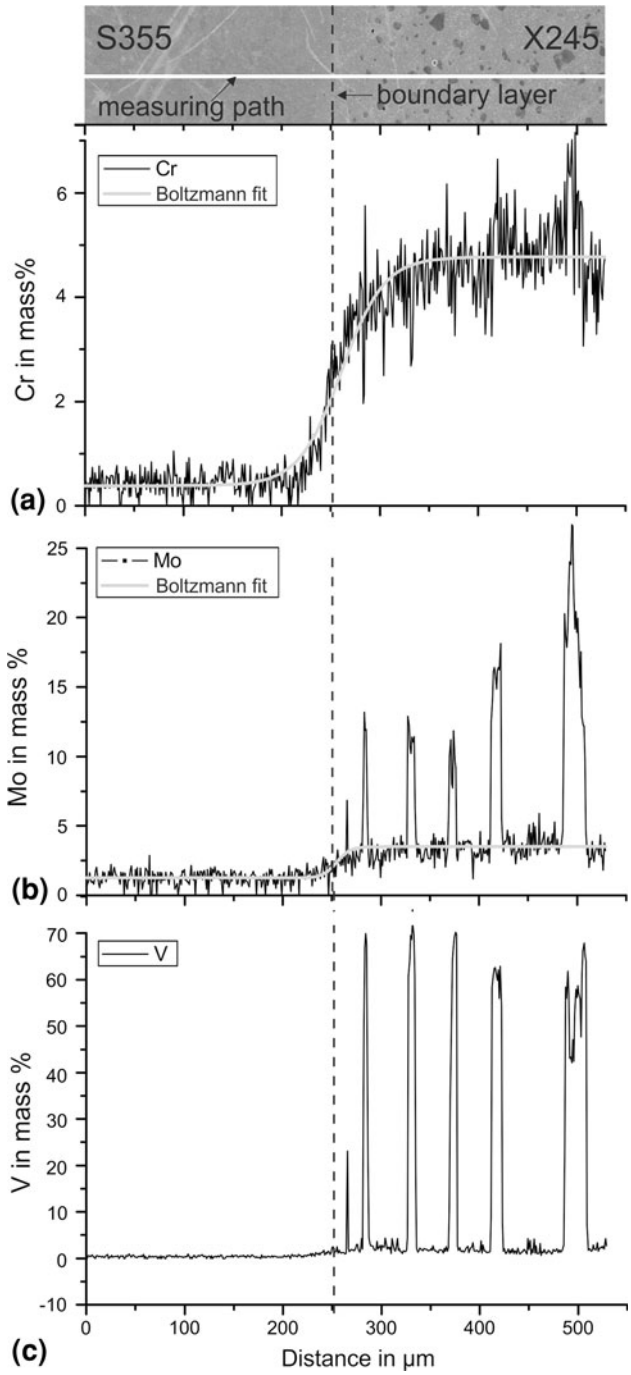

Fig. 9 Element linescan of the bond between coating and substrate materials (sample sintered at 1300 °C): (a) linescan of chromium, (b) linescan of molybdenum, and (c) linescan of vanadium

3.4 Diffusion Calculations and Computational Thermodynamics

Based on the known chemical compositions of substrate and coating materials (see Table 1) diffusion profiles for the composite were calculated using DICTRA. One major scope of the investigations was set to the diffusion of carbon as carbon cannot be quantified via EDX. However, carbon plays a leading role in matrix hardening which could explain the observed increase of hardness in the substrate material (see Fig. 8).The first step was to compare the calculated diffusion profiles of chromium and molybdenum to the EDX measurements. Figure 10(a) and (b) shows the calculated diffusion profiles for chromium and molybdenum which are in a good agreement with the EDX measurements and the Boltzmann fits (see Fig. 9). This indicates the good agreement of the simulation with the experimental results.

Figure 11(a) presents the calculated diffusion profile of carbon for a composite after 30 min dwell at 1280 °C. The results show a diffusion zone with a width of 3 mm. While the carbon drop in the coating material starts in a distance of 1 mm from the boundary layer, the calculated carbon increase in the substrate reaches to a depth of 2 mm. The overall carbon content was calculated to recognize the carbon diffusion of every phase. The detailed view of the diffusion zone (Fig. 11b) shows a decarburization starting from about 2.55 mass.% carbon in the bulk material (1 mm distance to boundary) to about 2.25 mass.% close to the boundary layer (0.01 mm). The diffusion gradient increases strongly with decreasing distance to the boundary layer. Within the substrate, there is an increase of the carbon content to a total level of 0.35 mass.% in close proximity of the boundary, which slowly drops to bulk values with increasing distance. A comparison with the hardness measurements (see Fig. 8) shows that the increase in hardness

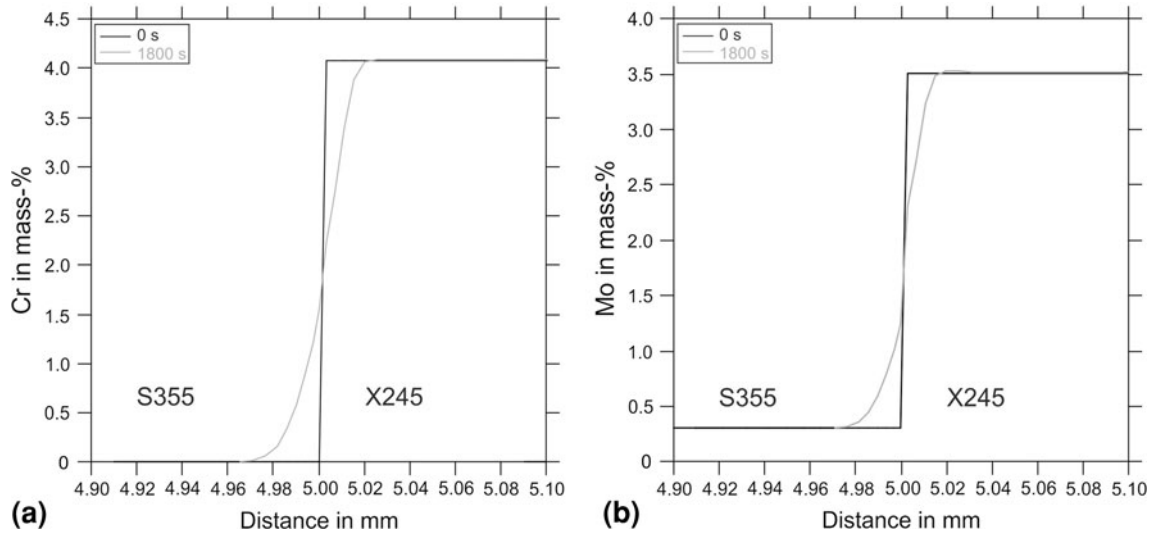

Fig. 10 Calculated diffusion profiles obtained by means of diffusion calculations: (a) Cr in mass.% and (b) Mo in mass.%

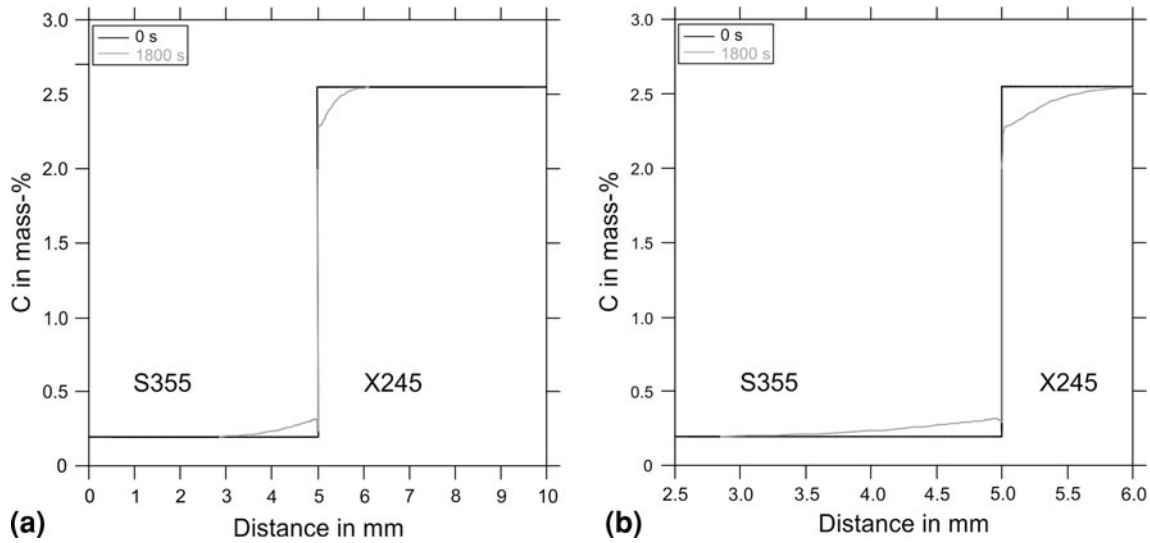

Fig. 11 Calculated diffusion profiles obtained by means of diffusion calculations: (a) C in mass.% (b) C in mass.%; detail of (a)

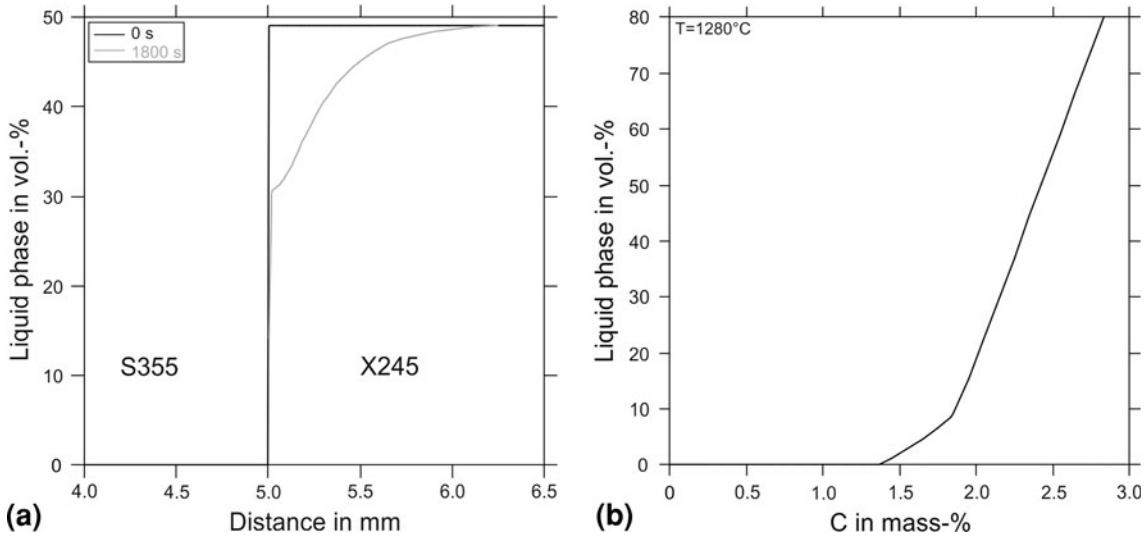

Fig. 12 Calculated volume fraction of liquid phase obtained by means of diffusion calculations and computational thermodynamics: (a) liquid phase in vol.% depending on the distance of the bond and (b) liquid phase in vol.% depending on the total amount of carbon

can be directly related to the diffusion of carbon in range up to 2 mm, which is also in agreement with the microstructural investigations (see Fig. 5). Carbon promotes the formation of a perlitic microstructure which exhibits a higher hardness compared to the ferritic bulk material.

Although no microstructural changes can be seen, a distinct increase of hardness is measured in a distance of 25 µm next to the boundary layer. This effect cannot be explained by carbon diffusion, but it matches with the calculated and measured diffusion range (about 30 µm) of chromium and molybdenum. It is known that, beside the effect of carbon on the microstructure, both chromium and molybdenum provide solid solution strengthening (Ref 25), which explains this increase of the hardness.

Another important question to the process refers to the origin of the comparatively high residual porosity next to the boundary zone after sintering at 1280 °C (see Fig. 4a).

Using DICTRA, it is possible to calculate the amount of liquid phase depending on the distance to the substrate material. The result is depicted in Fig. 12(a) which reveals a decrease of nearly 20% of liquid phase in the forefront of the substrate material. Using Thermo-Calc, a calculation was performed to analyze the amount of liquid phase depending on the overall carbon content at 1280 °C. The results show that the amount of liquid phase is directly related to the overall carbon content of the material, an effect which is already known in the literature (Ref 26). The diffusion of carbon leads to an increase of the solidus temperature and thereby to a reduced formation of liquid phase next to the boundary which can be assumed to be the reason for the residual porosity.

4. Summary

The tests have proven the feasibility of the densification of a cold work tool steel X245 by SLPS to almost theoretical density. The production of a composite consisting of a low-alloyed construction steel and a high-alloyed coating material has been successfully achieved. The selected sintering temperatures allow a cold work tool steel coating with a thickness exceeding 20 mm without pores or carbide networks. This indicates, together with the distinct diffusion zone between cladding material and substrate, the high quality of the bond.

Owing to the diffusion of alloying elements from X245 into the substrate, a zone of 10 µm thickness arises next to the boundary that is free of carbides. In the substrate, this carbon leads to an accelerated formation of perlite to a depth of 2 mm, which also leads to a increase of hardness in this area. In a greater distance from the boundary zone, the uninfluenced microstructure of S355 can be seen, consisting of a mixture of ferrite and perlite. The existence of pores at the interface after sintering at 1280 °C can also be explained by the diffusion of carbon into the substrate. Thermodynamic calculations revealed that the diffusion of carbon leads to a decrease of the liquid phase content to less than 20 vol.% next to the boundary layer.

References

1. A. Ißleib, A. Friedel, and I. Lubojanski, Verbundgießen für Verschleißteile—Stand und Zukunftsaussichten, *Gießerei-Praxis*, 1995, **7/8**, p 146–150
2. K.B. Arnold, T. Heijkoop, G.P. Lloyd, G. Rubenis, and I. Sare, Wear of Cast-Bonded Components in a Coal Pulveriser Mill, *Wear*, 1997, **203-204**, p 663–670
3. A. Lange, Verbundgießen für Anwendungen in der Verschleißtechnik, Ph.D. thesis, Otto-von-Guericke-Universität Magdeburg
4. A. Fischer, Hartlegierungen auf Fe-Cr-C-B Basis für die Auftragschweißung, *VDI, Zeitschrift*, 1985, **127**(9), p 323–324
5. C. Nissel, Stoffverbunde und Verbundbauteile durch heißisostatisches Pressen (HIP), *Zeitschrift Werkstofftechnik*, 1985, **16**, p 129–134
6. W. Theisen, HIP Cladding of Tools, *The Use of Tool Steels: Experience and Research: Proceedings of the 6th International Tooling Conference*, vol. 1, J. Bergström, G. Fredrikkson, M. Johansson, O. Kotik, and F. Thuvander, Eds., Sep 10-13, 2002 (Motala Grafiska), 2002
7. E. Bayer and H. Seilstorfer, HIP-Werkstofftechnik in der Kunststoffverarbeitung, *Metall*, 1991, **45**(10), p 1001–1006
8. P. Harlin and M. Olsson, Starch Consolidation of M3/2 High Speed Steel Powder—Influence of Process Parameters on Resulting Microstructure, *Powder Metall.*, 2007, **50**(4), p 345–353
9. S. Talacchia, I.J. San Martin, I. Urrutibeaskao, S. Jauregi, H.R. Palma, V. Martinez, and J. Urcola, Increasing Sintering Gate and Avoiding Grain Growth in High Speed Steels by Sintering in Nitrogen Rich Atmospheres, *Powder Metall.*, 1993, **36**(4), p 275–280

10. S. Giménez, C. Zubizarreta, V. Trabadelo, and I. Iturriza, Sintering Behaviour and Microstructure Development of T42 Powder Metallurgy High Speed Steel Under Different Processing Conditions, *Mater. Sci. Eng. A*, 2008, **480**(1-2), p 130–137
11. S. Weber, W. Theisen, F. Castro, and A. Pyzalla, Influence of Gas Atmosphere and Hard Particle Addition on the Sintering Behavior of High Alloyed PM Cold Work Tool Steels, *Mater. Sci. Eng. A*, 2009, **515**, p 175–182
12. H. Hill, S. Weber, S. Siebert, S. Huth, and W. Theisen, Comprehensive Investigations of the Super-Solidus Liquid-Phase Sintering of Two Plastic Mold Steels, *Metall. Mater. Trans. A*, 2010, **3**, p 686–695
13. D.J. Bolton and J.A. Gant, Microstructural Development and Sintering Kinetics in Ceramic Reinforced High Speed Steel Metal Matrix Composites, *Powder Metall. Metal Ceram.*, 1997, **40**(2), p 143–151
14. M.R. German, *Sintering Theory and Practice*, Wiley, New York, 1996
15. R.M. German, Rheological Model for Viscous Flow Densification During Supersolidus Liquid Phase Sintering, *Sci. Sinter.*, 2006, **38**(1), p 27–40
16. G. Petzow, *Metallographisches, Keramographisches, Plastographisches Ätzen*, 6th ed., Gebrüder Bornträger, Stuttgart, 1994
17. DIN EN ISO 6507-1: Metallische Werkstoffe—Härteprüfung nach Vickers—Teil 1: Prüfverfahren (2004)
18. A. Borgenstam, A. Engström, L. Höglund, and J. Agren, DICTRA, a Tool for Simulation of Diffusional Transformations in Alloys, *J. Phase Equilib.*, 2000, **21**(3), p 269–280
19. A. Schneider and G. Inden, Simulation of the Kinetics of Precipitation Reactions in Ferritic Steels, *Acta Mater.*, 2005, **53**, p 519–531
20. A.P. Silva, S. Weber, G. Inden, and R.A. Pyzalla, Influence of Hard Particle Addition and Chemical Interdiffusion on the Properties of Hot Extruded Tool Steel Compounds, *Mater. Sci. Eng. A*, 2009, **516**(1-2), p 193–200
21. Mob2, Mobility Database, Foundation of Computational Thermodynamics. Royal Institute of Technology, Stockholm (1999)
22. B. Jönsson, Assessment of the Mobility of Carbon in fcc C-Cr-Fe-Ni Alloys, *Zeitschrift für Metallkunde*, 1994, **85**(7), p 502–509
23. A. Engström and J. Agren, Assessment of Diffusional Mobilities in Face-Centered Cubic Ni-Cr-Al Alloys, *Zeitschrift für Metallkunde*, 1996, **87**(2), p 92–97
24. P. Franke and G. Inden, An Assessment of the Si Mobility and the Application to Phase Transformations in Silicon Steels, *Zeitschrift für Metallkunde*, 1997, **88**(10), p 795–799
25. H. Berns and W. Theisen, *Ferrous Materials—Steel and Cast Iron*, 1st ed., Springer, Berlin, 2008
26. R. Tandon, X.Y. Liu, and R.M. German, Role of Initial Powder Characteristics in Supersolidus Liquid Phase Sintering, *Adv. Powder Metall. Part. Mater.*, 1994, **3**, p 251–267